

Theory of fast ion–surface collisions at grazing incidence: emission of electrons due to capture and loss to the continuum

Uwe Thumm

Joint Institute for Laboratory Astrophysics, University of Colorado and National Institute of Standards and Technology, Boulder, CO 80309-0440, USA

Received 8 March 1991, in final form 15 October 1991

Abstract. Two mechanisms leading to the emission of electrons during the scattering of ions from a metal surface at grazing incidence are investigated. Emission probabilities are derived within a semiclassical approximation starting from first principles. For the capture of target electrons to the projectile continuum, first numerical results show three dominant features in the emitted electron spectrum. In addition to the Coulomb-cusp at zero relative velocity of electron and projectile, two structures with widths related to the Fermi energy of the metal conduction band are identified. They correspond to slow 'soft-collision' electrons and binary-encounter electrons, where the latter are most likely emitted at twice the projectile speed.

1. Introduction

During collisions with isolated atoms, passage through foils, or interactions with solid surfaces, energetic ions lead to the emission of electrons (Datz *et al* 1975, Berry *et al* 1985, Ferrariis and Baragiola 1986, Sánchez *et al* 1989, Winter *et al* 1989). The electron spectra show a peak where the velocity of the emitted electrons equals the projectile velocity. Mechanisms which lead to the emission of these electrons (usually referred to as cusp or convoy electrons) have been discussed by several authors (Macek 1970, Dettmann *et al* 1974, Belkić and Gayet 1975, Briggs and Day 1980, Jakubassa-Amundsen 1983, Burgdörfer 1986).

For gaseous targets, two mechanisms leading to cusp-electrons can be distinguished. For bare or nearly bare projectile ions, cusp-electrons result from the capture of target electrons into low-lying projectile continuum states, a process called electron capture to the continuum (ECC). The ECC cusp only occurs at small projectile scattering angles and is asymmetric with higher intensities on the low energy side. While the energy position and approximate form of the cusp is reproduced in the Born approximation (using Coulomb waves for the continuum states), the explanation of its asymmetry requires the inclusion of higher terms in the Born series (Shakeshaft and Spruch 1978, Macek *et al* 1981). The second mechanism, electron loss to the continuum (ELC), occurs if the projectile carries loosely bound electrons. As in the case of ECC, the position and approximate shape of the cusp for ELC are given in lowest-order perturbation theory, whereas its asymmetry only shows up in a higher-order description.

For solid targets, the mechanisms responsible for the emission of convoy electrons are not understood in detail (Sánchez *et al* 1989). In general, many charge exchange processes occur during the passage of the projectile through a foil. The convoy-electron yield depends sensitively on the foil thickness, the composition of the exit surface and the charge state and velocity of the projectile. According to Koschar *et al* (1987), the ELC process dominates during the passage of protons through carbon foils. Similarly, according to Schiwietz *et al* (1990), the ELC process, possibly enhanced by a collective transport mechanism, was found to dominate the convoy-electron yield during the passage of fast highly charged neon ions through thin carbon foils. Yamazaki and Oda (1984) argue that electrons set in motion inside the foil propagate independently of the projectile towards the exit surface. Subsequently, under the influence of the surface potential, these nearly free electrons are captured into projectile continuum states. The surface dependence of the convoy-electron yield in beam-foil experiments has been confirmed by Sánchez *et al* (1989). The electron yield from the collision of 60 keV protons with sodium-covered aluminium foils shows a strong dependence on the degree of the sodium coverage.

The strong dependence on the exit surface motivates the investigation of electron emission during grazing incident beam-surface collisions, which probe the surface dependence in pure form. In such experiments with 40–340 keV protons colliding with aluminium and copper surfaces, convoy-electron peaks have been measured (Ferraris and Baragiola 1986, Strohmeier 1986, Winter *et al* 1989) which are significantly broader than in ion-atom and ion-foil geometries. In first calculations (Winter *et al* 1989), this broadening was traced to the non-Coulomb-like modification of the final-state interaction due to a dipole field produced by the projectile and its image charge.

In this paper, we derive analytical expressions for the ECC and ELC scattering amplitudes and electron emission probabilities for the scattering of fast ions at metal surfaces at grazing incidence. In the case of ECC, we discuss qualitative features of the numerically calculated differential emission probability and relate the results to corresponding phenomena in ion-atom collisions. In both cases the theoretical procedures are semiclassical and closely related to the well known impact parameter method used in the description of ion-atom collisions (Briggs 1977). The processes of ECC and ELC are considered separately in sections 2 and 3. Section 4 contains our summary and conclusions. Atomic units are used throughout.

2. Electron capture to the continuum

In formulating the scattering amplitude we assume that the projectile ion moves on a prescribed classical trajectory $R(t)$ with velocity $v(t)$ with respect to an arbitrary origin located in the electronic surface. A formal derivation of first- and higher-order approximations to the exact semiclassical scattering amplitude has been given before (Thumm and Briggs 1989b). In lowest-order perturbation theory the amplitude for an initial state $|\Phi_k(t)\rangle$ and a final state $|\Phi_q(t)\rangle$ is

$$f(k, q) = -i \int_{-\infty}^{\infty} dt \langle \Phi_q(t) | V_p(t) | \Phi_k(t) \rangle. \quad (1)$$

In contrast to ion-atom scattering, the target and laboratory frame of reference are identical here. In this frame the Galilei-shifted Coulomb-continuum state of the

projectile reads

$$\begin{aligned}\Phi_{\mathbf{q}}(t) &= \phi_{\mathbf{q}}(\mathbf{r}) \exp\{i\mathbf{v} \cdot (\mathbf{R} + \mathbf{r}) - i(\epsilon + \frac{1}{2}v^2)t\} \\ \phi_{\mathbf{q}}(\mathbf{r}) &= F(q) \exp\{i\mathbf{q} \cdot \mathbf{r}\} {}_1F_1[i\alpha, 1; iq\mathbf{r} - i\mathbf{q} \cdot \mathbf{r}]\end{aligned}\quad (2)$$

with the Sommerfeld parameter and normalization factor given by

$$\alpha \equiv \frac{Z_p}{q} \quad F(q) \equiv \frac{1}{(2\pi)^{3/2}} \Gamma(1 - i\alpha) \exp\left\{\pi \frac{\alpha}{2}\right\}.\quad (3)$$

The exponential factors in (2) contain the translational momentum $\mathbf{q} + \mathbf{v}$ and kinetic energy $\epsilon + \frac{1}{2}v^2$ of an electron moving with the projectile. The electron's coordinate vector, momentum and energy with respect to the projectile's centre of mass are \mathbf{r} , \mathbf{q} and ϵ . The choice of a fixed frame of reference for the target makes the projectile potential in (1) time-dependent. For an assumed structureless incident ion of charge Z_p , it is given by

$$V_p(t) = \frac{-Z_p}{|\mathbf{r}_T - \mathbf{R}(t)|}\quad (4)$$

where \mathbf{r}_T is the electron's coordinate vector in the target frame. We emphasize that in our model only the final-state interaction due to the projectile's Coulomb potential is included. This potential dominates at large electron-surface distances and its long-range behaviour is the origin of the ECC cusp.

To perform the time integral in (1) analytically we need to specify the ion trajectory. The most convenient choice is a broken straight line trajectory (figure 1). Such a trajectory is assumed to be a sufficiently realistic representation of the specular reflection of an ion at grazing incidence and no fundamentally new effects would be expected from a more exact description of the classical motion. For a coordinate system with the x - y plane in the surface, the positive z -axis along the surface normal towards the vacuum and the positive x -axis along the projected projectile motion in the surface plane, this trajectory is parameterized by

$$\begin{aligned}\mathbf{R}(t) &= b\hat{e}_z + \mathbf{v}_{\pm}t \\ \mathbf{v}(t) &= v_{\parallel}\hat{e}_x \pm v_{\perp}\hat{e}_z =: \mathbf{v}_{\pm}\end{aligned}\quad (5)$$

such that $\mathbf{v} = \mathbf{v}_{-} = (v_{\parallel}, 0, -v_{\perp})$ on the incident half of the trajectory ($t < 0$), and $\mathbf{v} = \mathbf{v}_{+} = (v_{\parallel}, 0, v_{\perp})$ on the outgoing half ($t > 0$). The distance b of closest approach to the electronic surface (i.e. the 'jellium edge' located at $z = 0$) depends on v_{\perp} and is considered as a parameter of the theory. It is intuitively clear that quantitative predictions of a lowest-order theory strongly depend on b and the form of the trajectory. Qualitative results have been found to be insensitive to variations of b within a reasonable range.

In an attempt to estimate the distance b_0 of closest approach to the uppermost layer of the lattice points we assumed large neutralization probabilities for the incident protons at the considered small v_{\perp} and calculated b_0 by averaging different interatomic potentials over a string (continuum-string model) or plane (continuum-plane model) of surface atoms (Lindhard 1965, Gemmel 1974). Both continuum-string and

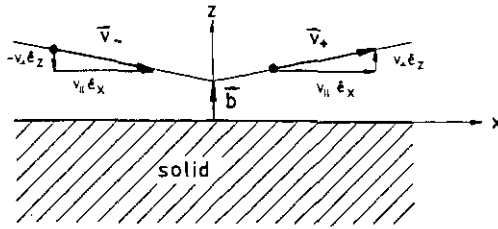


Figure 1. Coordinate system and model trajectory for $b > 0$ (special case where the projectile does not penetrate the electronic surface located at $z = 0$). The projectile velocity on the incoming and outgoing straight line segment is v_- and v_+ , respectively.

Table 1. The distance b_0 of closest approach to the uppermost layer of lattice points (in au) as a function of v_{\perp} , E_{\perp} or the angle of incidence α (as obtained for $v_{\parallel} = 2$) for hydrogen atoms incident on tungsten. Different interatomic potentials were used within the continuum-string and the continuum-plane model: screened Coulomb (sc), Thomas-Fermi (TF), Thomas-Fermi-Molière (TFM), Lindhard (L), and Biersack-Ziegler (BZ). Within the continuum-plane model the atoms are predicted to penetrate the solid at $v_{\perp} = 0.1$. For the Biersack-Ziegler potential, incident protons and the continuum-plane model (BZ-p) no penetration is predicted at $v_{\perp} = 0.1$.

v_{\perp} (au)	E_{\perp} (eV)	α	Continuum-string model			Continuum-plane model			
			sc	TF	TFM	TFM	L	BZ	BZ-p
0.1	249.8	2.9°	0.22	0.34	0.35	—	—	—	0.32
0.05	62.4	1.4°	0.44	0.79	0.80	0.25	0.24	0.64	2.70
0.02	10.0	0.6°	0.77	2.13	1.94	1.37	2.06	2.56	6.71
0.01	2.5	0.3°	1.03	4.12	2.82	2.27	8.18	3.62	9.97

continuum-plane potentials decrease monotonically with increasing distance from the surface. For a given energy $E_{\perp} = \frac{1}{2} M v_{\perp}^2$ perpendicular to the surface of a projectile of mass M , b_0 is given by the distance where this (asymptotic) energy is completely transformed into potential energy in the field of the string or plane. It is related to b by $b \approx b_0 - d/2$, where d is the lattice constant. The results for b_0 in table 1 show a strong dependence on the model (string or plane) and the underlying internuclear potential (screened Coulomb (with a screening constant given by the inverse of the Thomas-Fermi screening radius), Thomas-Fermi-Molière, Lindhard (as defined in Gemmell 1974) or Biersack-Ziegler (Biersack and Ziegler 1982, Ziegler *et al* 1985)). The hetero-nuclear Biersack-Ziegler potential was obtained by applying the geometric mean rule to the two homonuclear potentials V_1 and V_2 according to

$$V_{12} = \text{sign}(V_1 V_2) \sqrt{|V_1 V_2|}.$$

For $v_{\perp} = 0.1$ the perpendicular energy $E_{\perp} = 249.8$ eV clearly exceeds the critical energy for hydrogen penetration into the tungsten surface. The representation of this feature was found to be qualitatively correct only in the continuum-plane model. For the Biersack-Ziegler potential we further calculated b_0 assuming no neutralization of the protons before being reflected at the surface (column BZ-p in table 1). As one would expect, the absence of the screening hydrogen electron results in a stronger repulsive potential and larger values for b_0 .

In table 2 we show critical perpendicular velocities and energies for the penetration of hydrogen atoms and protons into a tungsten surface calculated within the continuum-plane model and different interatomic potentials. As in table 1, for the Biersack-Ziegler potential, we compare the two limiting cases, neutralization (BZ) and no neutralization (BZ-p), and find higher critical values for the latter.

Table 2. Critical perpendicular velocities and energies for the penetration of hydrogen atoms into a tungsten surface for different interatomic potentials (as explained in table 1) within the continuum-plane model, as well as results for incident protons (BZ-p).

	TFM	L	BZ	BZ-p
v_{\perp} (au)	0.068	0.069	0.090	0.12
E_{\perp} (eV)	114.3	120.5	201.6	335.5

For the broken line trajectory (5) we can perform the time integration separately for the incident and outgoing trajectory. To guarantee the correct scattering boundary conditions we include the convergence factor $\exp(-\delta|t|)$, $\delta \rightarrow 0^+$ in (1). The result can be written as

$$f(\mathbf{k}, \mathbf{q}) = i(2\pi)^{-3/2} Z_p F^*(q) \int d\mathbf{p} \tilde{\phi}_{\mathbf{k}}(\mathbf{p}) I(\mathbf{p}, \mathbf{q}, \mathbf{v}, \mathbf{k}) \exp\{i\mathbf{p} \cdot \mathbf{b}\}$$

$$I(\mathbf{p}, \mathbf{q}, \mathbf{v}, \mathbf{k}) \equiv I^-(\mathbf{p}, \mathbf{q}, \mathbf{v}_-, \mathbf{k}) + I^+(\mathbf{p}, \mathbf{q}, \mathbf{v}_+, \mathbf{k})$$

$$I^{\pm}(\mathbf{p}, \mathbf{q}, \mathbf{v}_{\pm}, \mathbf{k}) \equiv \mp \frac{A^{\pm}(\mathbf{p}, \mathbf{q} + \mathbf{v}_{\pm}) \exp\{\mp i\mathbf{v}_{\pm} \cdot \mathbf{b}\}}{\mathbf{p} \cdot \mathbf{v}_{\pm} + \epsilon - \frac{1}{2}v^2 - \epsilon_k \pm i\delta} \tag{6}$$

$$A^{\pm}(\mathbf{p}, \mathbf{q} + \mathbf{v}_{\pm}) \equiv \int d\mathbf{r} {}_1F_1[-i\alpha, 1; -i\mathbf{q}\mathbf{r} + i\mathbf{q} \cdot \mathbf{r}] \frac{1}{r} \exp\{i(\mathbf{p} - \mathbf{q} - \mathbf{v}_{\pm}) \cdot \mathbf{r}\}.$$

Using an integral representation of the confluent hypergeometric function (Abramowitz and Stegun 1970)

$${}_1F_1[-i\alpha, 1; -i\mathbf{q}\mathbf{r} + i\mathbf{q} \cdot \mathbf{r}] = [\Gamma(-i\alpha)\Gamma(1+i\alpha)]^{-1}$$

$$\times \lim_{\eta \rightarrow 0^+} \int_0^1 d\tau \tau^{-i\alpha-1+\eta} (1-\tau)^{i\alpha-\eta} \exp\{-i(\mathbf{q}\mathbf{r} - \mathbf{q} \cdot \mathbf{r})\tau\} \tag{7}$$

and the convergence factor $\exp(-\rho r)$, $\rho \rightarrow 0^+$, we obtain a representation of A^{\pm} in terms of an one-dimensional integral,

$$A^{\pm} = [\Gamma(-i\alpha)\Gamma(1+i\alpha)]^{-1} \lim_{\eta \rightarrow 0^+} \int_0^1 d\tau \tau^{-i\alpha-1+\eta} (1-\tau)^{i\alpha-\eta}$$

$$\times \lim_{\rho \rightarrow 0^+} \int d\mathbf{r} \exp\{i(\mathbf{p} - \mathbf{v}_{\pm} + [\tau - 1]\mathbf{q}) \cdot \mathbf{r}\} \frac{1}{r} \exp\{-i\mathbf{q}\tau\mathbf{r} - \rho r\}$$

$$= \lim_{\eta \rightarrow 0^+} \frac{4\pi}{[\Gamma(-i\alpha)\Gamma(1+i\alpha)][\mathbf{p} - \mathbf{v}_{\pm} - \mathbf{q}]^2} \int_0^1 d\tau \frac{\tau^{-i\alpha-1+\eta} (1-\tau)^{i\alpha-\eta}}{1 + B^{\pm}\tau} \tag{8}$$

where

$$B^\pm \equiv 2 \frac{(\mathbf{p} - \mathbf{v}_\pm - \mathbf{q}) \cdot \mathbf{q}}{(\mathbf{p} - \mathbf{v}_\pm - \mathbf{q})^2}.$$

At this point the initial states $|\Phi_{\mathbf{k}}\rangle$ are not yet specified and the scattering amplitude is expressed in terms of an integration over the initial state momentum distribution in (6) and the τ -integral in (8). Under the assumption that large momentum components of the initial state yield negligible contributions to (1) (as is true for the jellium initial state discussed later) in the high parallel velocity limit $|B^\pm| < 1$ holds and (Erdélyi 1953)

$$\begin{aligned} A^\pm &= \frac{4\pi}{(\mathbf{p} - \mathbf{v}_\pm - \mathbf{q})^2} {}_2F_1[1, -i\alpha; 1; -B^\pm] \\ &= \frac{4\pi}{(\mathbf{p} - \mathbf{v}_\pm - \mathbf{q})^2} (1 + B^\pm)^{i\alpha}. \end{aligned} \quad (9)$$

The τ -integral in (8) expresses the interaction of the projectile charge with the emitted electron in the continuum. This is easily seen by replacing the Coulomb wave in (1) by a plane wave describing the free motion of the emitted electron. In this case A^\pm is simply given by the Fourier transform of the Coulomb operator $1/r$,

$$A^\pm = \frac{4\pi}{(\mathbf{p} - \mathbf{q} - \mathbf{v}_\pm)^2} \quad (10)$$

and the normalization factor $F(q)$ in (6) is replaced by $(2\pi)^{-3/2}$.

2.1. Specification of initial states

Electron distributions inside a metal have been described self-consistently within the local density functional approximation (Lang and Kohn 1970, Lang 1973). In this model the ion cores are represented as a constant, 'smeared out' positive 'background charge'. The electronic many-body problem is reduced to the iterative solution of a one-electron Schrödinger equation with an effective potential. Apart from details (Friedel oscillations, formation of a surface dipole layer) the dominant features of this potential are translational invariance within the surface plane and a step-like increase along the positive z -axis. In the jellium model this effective potential is further approximated by a step potential. The conduction-band electrons are considered to be essentially free inside the metal; however, they are bound to the metal half space by the potential step $V_0 = \epsilon_F + W$. At zero temperature all states up to the Fermi level ϵ_F are occupied. An electron at ϵ_F needs the energy W (work function) to be released. Jellium states are conveniently labelled by the momentum \mathbf{k} . At zero temperature they lie within a sphere of radius $k_F = \sqrt{2\epsilon_F}$ in \mathbf{k} -space with a density of states $\rho = V/4\pi^3$ corresponding to a free electron gas and including a factor two for the spin degrees of freedom. The quantization volume V of the metal electrons is assumed to tend to infinity and none of the final expressions (the neutralization probabilities) depends on it. Even though the jellium model gives a poor description of the metal surface, it is adequate for our purpose since any detailed surface structure is averaged out in fast grazing incidence collisions due to the large

collision time (small v_{\perp}) during which the projectile passes over many surface atoms (large v_{\parallel}).

The momentum distribution of the jellium electrons is given by (Thumm and Briggs 1989b)

$$\begin{aligned}\tilde{\phi}_{\mathbf{k}}(\mathbf{p}) &= \delta^{(2)}(\mathbf{k}_{\parallel} - \mathbf{p}_{\parallel}) \tilde{u}_{k_z}(p_z) \\ \tilde{u}_{k_z}(p_z) &= \sqrt{\frac{2\pi}{V}} i \left\{ \frac{1}{p_z - k_z + i\delta} + \frac{R}{p_z + k_z + i\delta} - \frac{T}{p_z - i\gamma} \right\}\end{aligned}\quad (11)$$

where

$$\gamma \equiv \sqrt{2V_0 - k_z^2}.$$

The reflection and transmission coefficients are

$$R \equiv \frac{k_z - i\gamma}{k_z + i\gamma} \quad T \equiv \frac{2k_z}{k_z + i\gamma}.$$

The convergence factor δ accounts for the infinite extension of the target along the negative z -axis.

We consider fast ion-surface collisions at grazing incidence for which v_{\parallel} is larger than k_F such that (9) holds. With (9) and the initial states given by (11) the scattering amplitude can be summarized as

$$\begin{aligned}f(\mathbf{k}, \mathbf{q}) &= i(2\pi)^{-3/2} Z_P F^*(q) \int dp_z \tilde{u}_{k_z}(p_z) (I^- + I^+) \exp\{ip_z b\} \\ I^{\pm} &= \mp \frac{A^{\pm}}{\pm p_z v_{\perp} - \frac{1}{2}(k'_{\parallel}{}^2 + k_z^2 + v_{\perp}^2) + V_0 + \epsilon \pm i\delta} \exp\{\mp i v_{\perp} b\} \\ A^{\pm} &= \frac{4\pi}{(k'_{\parallel} - q_{\parallel})^2 + (p_z \mp v_{\perp} - q_z)^2} (1 + B^{\pm})^{i\alpha} \\ B^{\pm} &\equiv 2 \frac{(k'_{\parallel} - q_{\parallel}) \cdot q_{\parallel} + (p_z \mp v_{\perp} - q_z) q_z}{(k'_{\parallel} - q_{\parallel})^2 + (p_z \mp v_{\perp} - q_z)^2} \\ k'_{\parallel} &\equiv k_{\parallel} - v_{\parallel}.\end{aligned}\quad (12)$$

The three terms in (11) describe the incident, reflected and transmitted parts of the metal-electron wavefunction. The corresponding probability densities are well localized in p -space such that all the momentum components in (12) are practically limited to finite values. Thus, for large v_{\parallel} , B^{\pm} behaves as $1/v_{\parallel}$. Therefore, emphasizing the qualitative aspects of the capture process while keeping the numerical effort reasonably small, we replace the factor with the exponent $i\alpha$ by 1. This replacement is equivalent to an approximation made in the projectile final state (2). However, we want to emphasize that our calculation still includes the main physical effect of the projectile's Coulomb potential on the active electron, i.e. the Coulomb cusp, through the normalization constant F in (12). In this high parallel velocity approximation the p_z -integration can be performed analytically by contour integration. The contributions f^- and f^+ to the scattering amplitude from the incoming and outgoing trajectories are treated separately and the two cases of $b > 0$ (the ion does not penetrate the electronic surface defined by the jellium edge) and $b < 0$ (penetration) are distinguished.

2.2. Non-penetrating ions

For $b > 0$ the contour is closed in the upper p_z half plane, where f^- and f^+ each have two simple poles. The result of the p_z integration can be written as

$$f^\pm(\mathbf{k}, \mathbf{q}) = 2\pi i C \{ \text{Res}(i\gamma) + \text{Res}(a^\pm + id) \} \exp\{\mp i v_\perp b\} \quad (13)$$

with the residues (up to a constant) of the integral in (12) given by

$$\text{Res}(i\gamma) = -i T \sqrt{\frac{2\pi}{V}} \frac{\exp\{-\gamma b\}}{((i\gamma - a^\pm)^2 + d^2)(i\gamma \pm \Delta/v_\perp)}$$

$$\text{Res}(a^\pm + id) = \tilde{u}_{k_z}(a^\pm + id) \frac{\exp[(ia^\pm - d)b]}{2id(a^\pm + id \pm \Delta/v_\perp)}$$

and

$$C \equiv 2 \frac{Z_P}{v_\perp} F^*(q)$$

$$a^\pm \equiv q_z \pm v_\perp$$

$$d \equiv |\mathbf{k}'_\parallel - \mathbf{q}_\parallel|$$

$$\Delta \equiv V_0 + \epsilon - \frac{1}{2}(k'_\parallel{}^2 + k_z^2 + v_\perp^2).$$

Regarded as a function of b the amplitude has a bi-exponentially decaying form also found in the description of radiative ion-surface collisions (Thumm and Briggs 1989a),

$$f(\mathbf{k}, \mathbf{q}) = a_1 \exp\{-db\} + a_2 \exp\{-\gamma b\}.$$

The term with the decay constant d reflects the momentum matching condition $k'_\parallel = q_\parallel$ for the parallel motion of the active electron in the initial and final states. The second term reflects the exponentially decreasing jellium electron density outside the surface.

2.3. Penetrating ions

For $b < 0$ the ions may still be reflected at the topmost lattice plane situated half a lattice constant below the jellium edge. The integration contour has to be closed in the lower half plane, where f^- and f^+ each have four simple poles. In analogy to (13) we obtain

$$f^\pm(\mathbf{k}, \mathbf{q}) = -2\pi i C \{ \text{Res}(k_z - i\delta) + \text{Res}(-k_z - i\delta) \\ + \text{Res}(a^\pm - id) + \text{Res}(\mp \Delta/v_\perp - i\delta) \} \exp\{\mp i v_\perp b\} \quad (14)$$

where

$$\text{Res}(k_z - i\delta) = i \sqrt{\frac{2\pi}{V}} \frac{\exp\{ik_z b\}}{[(k_z - a^\pm)^2 + d^2](k_z \pm \Delta/v_\perp)}$$

$$\text{Res}(-k_z - i\delta) = i R \sqrt{\frac{2\pi}{V}} \frac{\exp\{-ik_z b\}}{[(k_z + a^\pm)^2 + d^2](-k_z \pm \Delta/v_\perp)}$$

$$\text{Res}(a^\pm - id) = i \tilde{u}_{k_z}(a^\pm - id) \frac{\exp[(ia^\pm + d)b]}{2id(a^\pm - id \pm \Delta/v_\perp)}$$

$$\text{Res}(\mp \Delta/v_\perp - i\delta) = \tilde{u}_{k_z}(\mp \Delta/v_\perp) \frac{\exp[\mp i \Delta/v_\perp b]}{(a^\pm \pm \Delta/v_\perp)^2 + d^2}.$$

The amplitude becomes singular with respect to q for perfect parallel momentum matching of initial and final state. The position of these singularities depends on k such that they are smeared out after an integration over all conduction-band states. In contrast to these singularities the 'Coulomb singularity' produced by the factor F in C is not influenced by the integration over the initial states.

2.4. Limiting case of a straight-line trajectory parallel to the surface

For $v_{\perp} \rightarrow 0$, the principal contributions to I^- and I^+ (equation (6)) cancel and

$$\lim_{v_{\perp} \rightarrow 0} f(\mathbf{k}, \mathbf{q}) = -iZ_P F^*(q) \delta(\mathbf{k}_{\parallel} \cdot \mathbf{v}_{\parallel} + \epsilon - \frac{1}{2}v^2 - \epsilon_k) \times \int dp_z \tilde{u}_{k_x}(p_z) A(\mathbf{k}_{\parallel}, p_z; \mathbf{q} + \mathbf{v}_{\parallel}) \exp\{ip_z b\}. \quad (15)$$

The δ distribution is singular for certain $\epsilon = \frac{1}{2}q^2$. For small $v_{\perp} \neq 0$ these singularities are collisionally 'broadened' to peaks due to the projectile motion perpendicular to the surface. The width of these peaks increases with v_{\perp} in agreement with an uncertainty relation for collision time and the energy $\frac{1}{2}v_{\perp}^2$ of the perpendicular motion. For $q_x > 0$ the peaks are known as binary-encounter peaks in the electron spectra of ion-atom collisions. The peaks produced for $q_x < 0$ correspond to very slow emitted electrons which will be referred to as 'soft-collision electrons' and require small momentum transfers or larger impact parameters.

2.5. Emission probabilities

Figure 2 shows the emission probability differential with respect to initial and final state

$$\frac{d^2 P}{d\mathbf{k} d\mathbf{q}} = \rho |f(\mathbf{k}, \mathbf{q})|^2$$

as a function of the emitted electron's momentum component q_x along \hat{v}_{\parallel} for the system $p + W$ at grazing incidence ($v_{\parallel} = 2, v_{\perp} = 0.02$). The momentum components perpendicular to the scattering plane of the active electron in the initial and final state are $k_y = 0, k_z = 0.5$ and $q_y = q_z = 0$, respectively (note that \mathbf{k} is defined in the laboratory frame and \mathbf{q} in the projectile frame). The distance of closest approach has been determined within the continuum-plane model, in connection with the Lindhard interatomic potential. For the given system and perpendicular velocity this yields a distance of closest approach to the top layer of $b_0 = 2.06$ or $b = -0.94$ (table 1, the lattice constant for W is $d = 6$). Since b is negative, the proton is supposed to penetrate the electronic surface before it is reflected at the uppermost layer of lattice points.

The three curves in figure 2 correspond to initial states with different k_x , i.e. to conduction-band electrons with different velocity components along \hat{v}_{\parallel} . The peaks at $q_x \approx 1.6, 1.9$ and 2.3 correspond to binary-encounter electrons which are emitted in the forward direction of the projectile. Their speed in the laboratory frame is approximately $2v_{\parallel}$ which has a simple physical explanation in terms of an elastic reflection of metal electrons from the projectile as the projectile dives into the electronic surface. The soft-collision electrons are emitted with larger probabilities than the binary-encounter electrons. Their peaks are located at parallel momenta

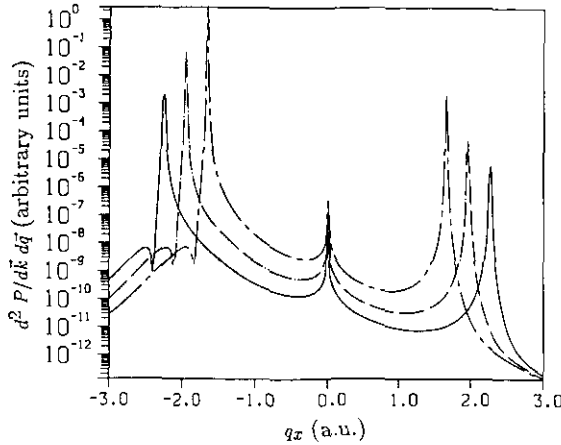


Figure 2. ECC emission spectrum differential in k and q for protons colliding with a tungsten surface at $v_{\parallel} = 2$, $v_{\perp} = 0.02$ as a function of the emitted electron parallel momentum q_x (defined in the projectile frame) with $q_y = q_z = 0$. Three different jellium initial states corresponding to conduction-band electrons moving in the scattering plane with different parallel momentum components are considered: $k_y = 0$, $k_z = 0.5$ and $k_x = -0.3$ (full curve); 0 (chain curve); 0.3 (broken curve). Every curve shows the secondary electron peak (left), the binary-encounter peak (right) and the Coulomb-cusp (at $q = 0$).

$q_x \approx -2.3$, -2 and -1.7 . The positions of these peaks and of the binary-encounter peaks are given as zeros of the argument of the δ function in (15). The soft-collision electrons are emitted at low velocities and are therefore expected to experience strong post-collisional interactions which are not included in the present model. It might be sufficient to include these interactions as image-charge effects, i.e. interactions of the active electron with its own and the projectile image charge. The third feature in figure 2 does not depend on the initial state. The location and form of the peak at $q_x \approx 0$ are given by the normalization factor $F(q)$ of the Coulomb final state (equation (2)). This factor is related to the long-range behaviour of the projectile's Coulomb potential. The $1/q$ singularity in this factor expresses the ability of the Coulomb potential to attract probability density from an infinite volume towards the projectile nucleus. It vanishes as soon as the potential is cut off at a fixed but arbitrarily large radius.

The differential emission probabilities in figure 2 show the physics incorporated in our first-order model in a qualitative way. No absolute values are given since quantitative results depend strongly on the distance b_0 which is, itself, sensitive to such model assumptions as the choice of an internuclear potential (cf table 1) and a broken straight-line projectile trajectory. In addition, especially for the emission of soft-collision electrons, we would not expect more than an order of magnitude estimate due to the limitation to first-order perturbation theory.

After integration over all initial states at zero temperature the emission probability, differential with respect to the momentum of the emitted electron, reads

$$\frac{dP}{dq} = \rho \int_{k \leq k_F} dk |f(\mathbf{k}, \mathbf{q})|^2. \quad (16)$$

Without actually carrying out the integration over the initial conduction-band states

numerically, we can infer, from the k -dependence of $dP/dk \, dq$ shown by the three curves in figure 2, that the main effect of this integration would result in a broadening of the soft-collision and binary-encounter peaks to structures of an approximate width of $2k_F$, whereas the Coulomb cusp at $q = 0$ is left unchanged.

3. Electron loss to the continuum

In describing the process of electron loss to the continuum we assume that a metal electron has been captured on the incoming part of the trajectory into a bound state of the projectile at a relatively large ion-surface distance. While the projectile is specularly reflected at the surface, the supposed hydrogenic projectile loses its electron to a continuum state of projectile and target. Due to the slow projectile motion perpendicular to the surface (grazing incidence), the target strongly influences the active electron, even at high projectile energies. Unlike the situation in fast ion-atom collisions the description of the final state as a Coulomb state, i.e. the neglect of the target's influence, is not appropriate here. We therefore include target interactions due to an image charge induced by the projectile nucleus. The total final-state interaction is then due to a dipole formed by the projectile nucleus and its image charge. The different threshold behaviour of dipole and Coulomb states is finally responsible for the larger width of the dipole cusp as was observed in recent experiments (Ferrariis and Baragiola 1986, Winter *et al* 1989) and discussed before by Winter *et al* (1989). In this section we outline a perturbative theory for ELC. As in section 2, the projectile is assumed to move along a classical trajectory.

The initial and final asymptotic states belong to different channel Hamiltonians H_i and H_f . The initial asymptotic state $|\Phi_i(t)\rangle$ is a bound eigenstate of the projectile Hamiltonian $H_i = K + V_P$, where K and V_P denote the kinetic energy operator and the projectile-nucleus Coulomb potential. The final asymptotic state is the dipole state $|\Psi_{\text{dip}}(t)\rangle$ which is an eigenstate of the final channel Hamiltonian $H_f = K + V_{\text{dip}}$. The dipole potential is the sum of V_P and the image potential $V_{\text{nuc}}^{\text{im}}$ of the projectile nucleus,

$$V_{\text{dip}} = V_P + V_{\text{nuc}}^{\text{im}}.$$

The total Hamiltonian is

$$\begin{aligned} H &= H_i + V_i = H_f + V_f \\ &= K + V_P + V_J + V_{\text{nuc}}^{\text{im}} + V_{\text{el}}^{\text{im}} \end{aligned}$$

where V_J is the surface potential assumed to be a simple potential step of height V_0 at the electronic surface (jellium model). The perturbative potential in the initial channel is

$$V_i = V_J + V_{\text{nuc}}^{\text{im}} + V_{\text{el}}^{\text{im}}$$

where $V_{\text{el}}^{\text{im}}$ is the image potential of the active electron. In the final channel the perturbative potential V_f includes V_J and $V_{\text{el}}^{\text{im}}$. It is assumed to be steady, such that

$$\begin{aligned} V_f &= \begin{cases} -V_0 & z \leq z_0 \\ V_{\text{el}}^{\text{im}} & z > z_0 \end{cases} \\ V_{\text{el}}^{\text{im}} &= -\frac{1}{4z} & z_0 = \frac{1}{4V_0}. \end{aligned}$$

The steady connection of V_j and V_{el}^{im} strictly speaking requires a modification of the potentials at small z . At small z , however, V_{el}^{im} as defined here loses its meaning as a description of the collective response of the metal–electron gas to the external electron.

The dipole potential induces a local enhancement of the electron probability density in the final channel within a cone that stands perpendicularly on the surface (such that the projectile lies on its symmetry axis) and opens towards the vacuum. The theory of final-state interaction (Gillespie 1964, Taylor 1972) describes this redistribution through an ‘enhancement factor’ equal to the reciprocal value of the Jost function. For the spherically symmetric, asymptotic potential

$$V_{dip} \approx \begin{cases} -2R(t)/r^2 & r > r_0 \\ -2R(t)/r_0^2 & r \leq r_0 \end{cases}$$

the Jost function to the l th partial wave reads

$$\mathcal{F}_l(q, R(t)) = 1 + \frac{2}{q} \int_0^\infty dr \hat{h}_l^+(qr) V_{dip}(r) \varphi_l(q, r). \quad (17)$$

The asymptotic behaviour of the Riccati–Hankel function is

$$\lim_{z \rightarrow \infty} \hat{h}_l^+(z) = \exp\{iz - il\pi/2\}.$$

The normalization of the regular solution φ_l to the radial equation is given by

$$\lim_{r \rightarrow 0} \varphi_l(q, r) = \hat{j}_l(qr).$$

The Riccati–Bessel function behaves for small arguments as

$$\hat{j}_l(z) \approx \frac{z^{l+1}}{(2l+1)!}.$$

Close to threshold (small q) scattering is dominated by s-wave contributions. For constant dipole potential strength the dipole wavefunction can then be separated (Taylor 1972) into the enhancement factor and a plane wave as

$$|\Psi_{dip}(t)\rangle \approx \frac{1}{\mathcal{F}_0(q, R)} |q(t)\rangle. \quad (18)$$

In fact, for grazing incidence collisions, the potential strength varies slowly in t due to the perpendicular motion of the projectile. In an adiabatic approximation we therefore replace R by $R(t)$ in (18).

To first order in V_f the semiclassical transition amplitude is

$$f = -i \int_{-\infty}^{\infty} dt \langle \Psi_{dip}(t) | V_f(t) | \Phi_i(t) \rangle. \quad (19)$$

With (18) it becomes

$$f(q) \approx -i \int_{-\infty}^{\infty} dt \frac{1}{\mathcal{F}_0(q, R(t))} \langle q(t) | V_f(t) | \Phi_i(t) \rangle. \quad (20)$$

Since both the potential and the overlap of the wavefunctions in (19) vanish quickly for increasing R , the loss process predominantly occurs close to the surface. Introducing the effective loss distance R_L , (20) can be further approximated by

$$f(q) \approx \frac{1}{\mathcal{F}_0(q, R_L)} f^{B1}(q) \quad (21)$$

where f^{B1} is the first-order transition amplitude for electron emission into the free final state $|q\rangle$. The amplitude f^{B1} can be expressed in terms of exponential integral functions and incomplete Γ functions. The Jost function in (21) can be calculated analytically (Gaillitis 1962, O'Malley 1965, Domcke and Cederbaum 1980, Estrada and Domcke 1984). The resulting expressions, however, are very unwieldy. Alternatively the integral in (17) and φ_l can be calculated numerically (the latter efficiently by using the Numerov method).

The threshold behaviour of the $l = 0$ dipole and Coulomb Jost function are identical. Equations (20) and (21) are therefore not suitable to describe the observed broadened cusp. They are, however, useful for an order-of-magnitude estimate of ELC emission probabilities. In order to describe not only the magnitude, but the 'wings' of the cusp as well, i.e. its width, higher angular momenta must be taken into account. Their threshold behaviour is given by

$$\frac{1}{|\mathcal{F}_l(q, R)|^2} = a(l)q^{-1+b(l)}$$

$$b(l) = 2\sqrt{(l + \frac{1}{2})^2 - D}$$

where the argument of the root is supposed to be positive, D is the dipole potential strength and the coefficient $a(l)$ gives the relative contribution of the l th partial wave.

The emission probability may be parametrized as

$$P = \frac{1}{|\mathcal{F}_0(q, R_L)|^2} |f^{B1}(q)|^2 (1 + Aq^B) \quad (22)$$

where the parameters A and $B > 0$ include the averaged contribution of partial waves with $l \neq 0$. After folding P with the detector resolution, R_L , A and B can be determined by fitting the result to measured spectra.

4. Summary and conclusions

We have outlined a semiclassical theory for electron emission in fast grazing incidence ion-surface collisions which is closely related to the impact parameter method, well known from the theory of fast ion-atom collisions. Modifications are due to the different symmetry and electronic structure of the target. While for ionic or atomic targets the initial states are bound, i.e. localized, we consider delocalized states of a metal conduction band and describe them as jellium states in a simple model. Furthermore, the classical projectile path is represented by one broken straight-line trajectory as opposed to a bundle of straight-line trajectories, each specified by an impact parameter, used in the case of gaseous targets. In the limiting case of zero perpendicular velocity the projectile moves along a straight line parallel to the surface

and the analytical expressions for the scattering amplitude become formally identical to the corresponding expressions for ion-atom collisions. The theory is Galilei-invariant and therefore includes kinematic level shifts in a natural way. It has been applied to two processes leading to the emission of delocalized metal electrons.

For electrons emitted from jellium states (ECC) we provide analytical expressions for the scattering amplitude in lowest-order perturbation theory. While the initial state resolved spectra show three peaks of different physical origin (soft-collision, cusp and binary-encounter electrons), two of these peaks, corresponding to soft-collision and binary-encounter electrons, are expected to broaden to structures of approximately twice the conduction-band width. The third peak (cusp electrons) is only related to the final state. Its shape, therefore, remains unchanged.

Within the same semiclassical framework we have outlined the theory for the emission of electrons (ELC) bound to the projectile, e.g. after being resonantly captured by the incident ion at large distances from the surface. The combined effect of the projectile nucleus and its induced image charge on the emitted electron is included in the form of a asymptotic dipole final-state interaction. Finally, approximations have been suggested which lead to the factorization of the scattering amplitude into a dipole-enhancement factor and the first-order amplitude for a free final state.

Measured ECC spectra are expected to show additional structures in the broadened soft-collision and binary-encounter peaks. These structures should be mainly related to the metal density of states and, to a much smaller extent, to the detailed structure of the metal electronic states (which are subject to average processes during the calculation of scattering amplitudes). The jellium model does not include this structure. However it could be accounted for by replacing in (16) the constant jellium density of states (in k -space) by a more realistic density-of-states function, derived either from surface electronic structure calculations or measurements (e.g. measured Auger spectra).

Recently, Mišković and Janev (1989) published a paper on the emission of conduction-band electrons due to Auger neutralization at grazing incidence proton-surface collisions. The calculated emitted electron energy distribution was shown to experience a strong increase in the peak position and width, with simultaneous decrease in the peak value, as the parallel velocity increased. For the highest considered parallel velocity of $v_{\parallel} \approx 1.9$, which is comparable to the value of $v_{\parallel} = 2$ we supposed in figure 2, the distribution of Auger electrons was found to cover a wide range of emitted electron energies. This range appears to be larger than the range of approximately $2k_F$ predicted in this paper for the distributions of soft-collision and binary-encounter electrons, such that for fast grazing incidence collisions, the emitted electron distributions corresponding to different emission mechanisms might be distinguished by their widths.

Acknowledgments

Stimulating discussions with J S Briggs, J T Broad and J Burgdörfer are gratefully acknowledged. This work was supported in part by NSF grant PHY90-12244 to the University of Colorado.

References

Abramowitz M and Stegun I 1970 *Handbook of Mathematical Functions* (New York: Dover)

- Belkić D and Gayet R 1975 *J. Phys. B: At. Mol. Phys.* **8** 442
- Biersack J P and Ziegler J F 1982 *Nucl. Instrum. Methods* **194** 93
- Berry S D *et al* 1985 *Phys. Rev. A* **31** 1392
- Briggs J S 1977 *J. Phys. B: At. Mol. Phys.* **10** 3075
- Briggs J S and Day M H 1980 *J. Phys. B: At. Mol. Phys.* **13** 4797
- Burgdörfer J 1986 *J. Phys. B: At. Mol. Phys.* **19** 417
- Datz S, Appleton B R, Biggerstaff J A, Noggle T S and Verbeek H 1975 *Oak Ridge National Laboratory Annual Report* p 107
- Dettmann K, Harrison K G and Lucas M W 1974 *J. Phys. B: At. Mol. Phys.* **7** 269
- Domcke W and Cederbaum L S 1980 *J. Phys. B: At. Mol. Phys.* **14** 149
- Erdélyi A (ed) 1953 *Bateman Manuscript Project* vol 1 (New York: McGraw-Hill) 2.12.1; 2.8.4
- Estrada H and Domcke W 1984 *J. Phys. B: At. Mol. Phys.* **17** 279
- Ferrariis L F and Baragiola R A 1986 *Phys. Rev. A* **33** 4449
- Gailitis M and Damburg R 1962 *Proc. R. Soc.* **82** 192
- Gemmell D S 1974 *Rev. Mod. Phys.* **46** 129
- Gillespie J 1964 *Final-State Interactions* (San Francisco: Holden-Day)
- Jakubassa-Amundsen D H 1983 *J. Phys. B: At. Mol. Phys.* **16** 1767
- Koschar P, Clouvas A, Heil D, Burkhard M, Kemmler J and Groeneveld K O 1987 *Nucl. Instrum. Methods* **24/25** 153
- Lang N D 1973 *Solid State Phys.* **28** 225
- Lang N D and Kohn W 1970 *Phys. Rev. B* **1** 4555
- Lindhard J 1965 *K. Dan. Vidensk. Selsk. Mat. Fys. Medd.* **34** no 4
- Macek J H 1970 *Phys. Rev. A* **1** 235
- Macek J H, Potter J E, Duncan M M, Menendez M G, Lucas M W and Steckelmacher W 1981 *Phys. Rev. Lett.* **46** 1571
- Mišković Z L and Janev R K 1989 *Surf. Sci.* **221** 317
- O'Malley T F 1965 *Phys. Rev. A* **137** 1668
- Sánchez E A, de Ferrariis L F and Suárez S 1989 *Nucl. Instrum. Methods B* **43** 29
- Schiwietz G, Biersack J P, Schneider D, Stolterfoht N, Fink D, Montemayor V J and Skogvall B 1990 *Phys. Rev. B* **41** 6262
- Shakeshaft R and Spruch L 1978 *Phys. Rev. Lett.* **41** 1037
- Strohmeier P 1986 *Diplomarbeit* Universität Münster
- Taylor J R 1972 *Scattering Theory* (New York: Wiley)
- Thumm U and Briggs J S 1989a *Nucl. Instrum. Methods* **40/41** 161; 1990 *Nucl. Instrum. Methods* **47** 476
- 1989b *Nucl. Instrum. Methods* **43** 471
- Winter H, Strohmeier P and Burgdörfer J 1989 *Phys. Rev. A* **39** 3895
- Yamazaki Y and Oda N 1984 *Phys. Rev. Lett.* **52** 29
- Ziegler J F, Biersack J P and Littmark U 1985 *The Stopping and Range of Ions in Solids* (New York: Pergamon)